

TIDALLY-DRIVEN ROCHE-LOBE OVERFLOW OF HOT JUPITERS WITH MESA

FRANCESCA VALSECCHI¹, SAUL RAPPAPORT², FREDERIC A. RASIO¹, PABLO MARCHANT³, LESLIE A. ROGERS⁴
Draft version August 24, 2018

ABSTRACT

Many exoplanets have now been detected in orbits with ultra-short periods, very close to the Roche limit. Building upon our previous work, we study the possibility that mass loss through Roche lobe overflow (RLO) may affect the evolution of these planets, and could possibly transform a hot Jupiter into a lower-mass planet (hot Neptune or super-Earth). We focus here on systems in which the mass loss occurs slowly (“stable mass transfer” in the language of binary star evolution) and we compute their evolution in detail with the binary evolution code MESA. We include the effects of tides, RLO, irradiation and photo-evaporation of the planet, as well as the stellar wind and magnetic braking. Our calculations all start with a hot Jupiter close to its Roche limit, in orbit around a sun-like star. The initial orbital decay and onset of RLO are driven by tidal dissipation in the star. We confirm that such a system can indeed evolve to produce lower-mass planets in orbits of a few days. The RLO phase eventually ends and, depending on the details of the mass transfer and on the planetary core mass, the orbital period can remain around a few days for several Gyr. The remnant planets have a rocky core and some amount of envelope material, which is slowly removed via photo-evaporation at nearly constant orbital period; these have properties resembling many of the observed super-Earths and sub-Neptunes. For these remnant planets we also predict an anti-correlation between mass and orbital period; very low-mass planets ($M_{\text{pl}} \lesssim 5 M_{\oplus}$) in ultra-short periods ($P_{\text{orb}} < 1$ d) cannot be produced through this type of evolution.

Subject headings: Planetary Systems: planet-star interactions—planets and satellites: gaseous planets—stars: evolution—stars: general—(stars:) planetary systems

1. INTRODUCTION

Hot Jupiters, giant planets in orbits of a few days, constitute one of the many surprises of exoplanet searches. Whether their tight orbits are the result of inward migration in a protoplanetary disk (Goldreich & Tremaine 1980; Lin et al. 1996; Ward 1997; Murray et al. 1998), or tidal circularization of an orbit made highly eccentric via gravitational interactions (Rasio & Ford 1996; Wu & Murray 2003; Fabrycky & Tremaine 2007; Chatterjee et al. 2008; Nagasawa et al. 2008; Wu & Lithwick 2011; Naoz et al. 2011; Plavchan & Bilinski 2013; Valsecchi & Rasio 2014a,b), is still matter of debate. Certainly, independent of the formation mechanism, tidal dissipation in the slowly-spinning host stars is causing the orbits of the tightest hot Jupiters currently known to shrink rapidly (e.g., Rasio et al. 1996; Sasselov 2003; Birkby et al. 2014; Valsecchi & Rasio 2014a; see also Table 1 in Valsecchi & Rasio 2014a and references therein).

Eventually, hot Jupiters may decay down to their Roche-limit separation. While it is commonly assumed that the planet is then quickly accreted

by the star (e.g., Jackson et al. 2009; Metzger et al. 2012; Schlaufman & Winn 2013; Damiani & Lanza 2014; Teitler & Königl 2014; Zhang & Penev 2014), for a typical system hosting a hot Jupiter orbiting a sun-like star the ensuing mass transfer (‘MT’) may be dynamically stable (Sepinsky et al. 2010). This was suggested, e.g., to explain WASP-12’s transit features (Lai et al. 2010). Trilling et al. (1998) investigated the possibility of halting inward disk migration through tides and Roche-lobe overflow (‘RLO’) MT from a hot Jupiter to a rapidly-spinning (young) stellar host. However, we note that the host stars of the tightest hot Jupiters are observed to be rotating slowly at present.

In Valsecchi et al. (2014), we investigated the fate of a hot Jupiter transferring mass to its stellar host using a simplified binary MT model. We showed that the planet could be stripped of its envelope, resulting in a hot super-Earth-type planet. This model naturally solves some of *Kepler*’s evolutionary puzzles (e.g., Kepler-78; Howard et al. 2013; Pepe et al. 2013; Sanchis-Ojeda et al. 2013), and it could explain the excess of isolated hot super-Earth- or sub-Neptune-size planets seen in the *Kepler* data (Steffen & Farr 2013).

Our previous work relied on several simplifying and potentially key assumptions. First, while using detailed models for the host star, we adopted published mass-radius relations for the planetary component, thus assuming that the planet remains in thermal equilibrium throughout the MT. Second, even though our planetary models included the effect of stellar irradiation on the planetary mass-radius relations, irradiation was kept *fixed*, while it is expected to vary as the orbit evolves during MT. Furthermore, we neglected the resulting mass

¹ Center for Interdisciplinary Exploration and Research in Astrophysics (CIERA), and Northwestern University, Department of Physics and Astronomy, Evanston, IL 60208, USA. FV: francesca@u.northwestern.edu; FR: rasio@northwestern.edu.

² Department of Physics, and Kavli Institute for Astrophysics and Space Research, Massachusetts Institute of Technology, Cambridge, MA 02139, USA, sar@mit.edu.

³ Argelander-Institut für Astronomie, Universität Bonn, Auf dem Hgel 71, D-53121 Bonn, Germany; pablo@astro.uni-bonn.de.

⁴ Department of Astronomy and Department of Geophysics and Planetary Sciences, California Institute of Technology, Pasadena, CA 91125, USA; larogers@caltech.edu.

loss due to photo-evaporation (Murray-Clay et al. 2009; Jackson et al. 2010; Lopez et al. 2012; Lopez & Fortney 2013; Owen & Alvarez 2015), even though various studies found it to play an important role in the evolution of highly irradiated super-Earth and sub-Neptune-type planets (e.g., Jackson et al. 2010; Rogers et al. 2011; Lopez et al. 2012; Batygin & Stevenson 2013; Lopez & Fortney 2013; Owen & Wu 2013).

As a natural continuation of our previous work, here we significantly expand upon our simple binary MT model to include detailed planetary evolution, as well as the effects of a varying irradiation and the consequent photo-evaporative mass loss from the planet. For these new calculations we utilize the Modules for Experiments in Stellar Astrophysics (MESA) evolution code (Paxton et al. 2011, 2013, 2015).

The plan of the paper is as follows. In Section § 2 we describe the stellar and planetary models used in this work. In Section § 3 we describe our orbital evolution model and the physical mechanisms entering the calculation. We present some examples of our orbital evolution calculations in Section 4 and discuss our results in Section 5. We conclude in Section 6.

For quick reference, the notations adopted in this work are summarized in Table 1.

Table 1
Definition of the main parameters used in this work.

| Parameter | Definition |
|---|--|
| M_*, M_{pl} | Mass |
| M_c, M_{env} | Planetary core and envelope mass |
| R_*, R_{pl} | Radius |
| $R_{\text{lobe},*}, R_{\text{lobe,pl}}$ | Roche-lobe radius |
| T_*, T_{pl} | Surface temperature |
| $\Omega_*, \Omega_{\text{pl}} (\Omega_o)$ | Spin (orbital) frequency |
| Z | Metallicity |
| a | Semimajor axis |
| P_{orb} | Orbital period |
| J_{orb} | Orbital angular momentum |
| $f = M_{\text{env}}/M_{\text{pl}}$ | Envelope mass fraction |
| $q = M_{\text{pl}}/M_*$ | Planet to star mass ratio |
| t, t_{MS} | Stellar age and main-sequence lifetime |

Note. — The subscripts “*” and “pl” refer to the star and planet, respectively. We take the stellar age to be equal to the system age and t_{MS} to be the age when the mass fraction of H at the center of the star drops below 10^{-15} .

2. STELLAR AND PLANETARY MODELS

The stellar and planetary models adopted in this work are computed with MESA (version 7184; Paxton et al. 2011, 2013, 2015). In particular, the planets are created and evolved closely following the test suite *make_planets* provided within MESA and the input files yielding Figure 3 of Paxton et al. (2013)⁵. In what follows we give specifications only for those MESA parameters that are changed from the values adopted in these input files.

⁵ available at <http://mesastar.org/results/mesa2/planets>

In all our calculations, we consider a $1 M_{\odot}$ star paired with a $1 M_J$ planet. We assume solar composition ($Y = 0.27, Z = 0.02$) for both the star and planet envelope, and keep the mixing length parameter α_{MLT} to MESA’s default value of 2. For the planet, we expand on our previous work (Valsecchi et al. 2014) and consider models with solid cores of masses $M_c = 1 M_{\oplus}, 5 M_{\oplus}, 10 M_{\oplus}, 15 M_{\oplus}$ and, $30 M_{\oplus}$. The initial model radius (required by the *create_initial_model* routine) was varied between $2-5 R_J$ to facilitate MESA’s convergence when creating the starting planetary model. For the cores, we use a constant density of 5 g cm^{-3} (following Batygin & Stevenson 2013) and we take the heat-flux arising from radioactive decay in the core to be zero (following the *make_planets* test suite).

We account for the effects of irradiation and photo-evaporation as follows. For irradiation, we use the $F_* - \Sigma_{\text{pl}}$ surface heating function. Here F_* is the day-side flux from the star at the substellar point, given by

$$F_* = \sigma T_*^4 \left(\frac{R_*}{a} \right)^2. \quad (1)$$

The planet equilibrium temperature, T_{eq} , is

$$T_{\text{eq}} = T_* \left(\frac{R_*}{2a} \right)^{1/2}, \quad (2)$$

(Saumon et al. 1996) so that the power received from the host star could be radiated away in equilibrium if the planet had this temperature over its entire surface. The parameter Σ_{pl} is the column depth reached by irradiation. Here we adopt a value of $\Sigma_{\text{pl}} = 1 \text{ g/cm}^2$, which yields planetary mass-radius relations in agreement with detailed models by Fortney et al. (2007), within a few percent for highly irradiated planets, as shown in Figure 1. We discuss the effect of varying Σ_{pl} in Section 4.2.3. In what follows, the planetary radius corresponds to an optical depth $\tau = 2/3$.

Irradiation leads to photo-evaporative (“PE”) mass loss from the planet. Specifically, this process is thought to be most efficient when a hot Jupiter is strongly irradiated by ultraviolet (UV) and X-ray photons, which photo-ionize atomic H in the planetary atmosphere. The resulting heat input, when high enough to induce temperatures corresponding to the escape velocity, can cause outflows. Murray-Clay et al. (2009) identified two regimes, based on the stellar flux F_{XUV} (however, see Owen & Alvarez 2015). For $F_{\text{XUV}} > 10^4 \text{ erg cm}^{-2} \text{ s}^{-1}$ the mass loss is “radiation/recombination” limited and it is described by

$$\dot{M}_{\text{rr-lim}} \sim 4 \times 10^{12} \left(\frac{F_{\text{XUV}}}{5 \times 10^5 \text{ erg cm}^{-2} \text{ s}^{-1}} \right)^{1/2} \text{ g s}^{-1}. \quad (3)$$

For $F_{\text{XUV}} \lesssim 10^4 \text{ erg cm}^{-2} \text{ s}^{-1}$ the mass loss is “energy limited” and it is described by (Erkaev et al. 2007; Lopez et al. 2012)

$$\dot{M}_{\text{e-lim}} \approx \frac{\epsilon \pi F_{\text{XUV}} R_{\text{XUV}}^3}{GM_p K_{\text{tide}}}, \quad (4)$$

where $K_{\text{tide}} = 1 - (3/2)(1/\xi) + (1/2)(1/\xi^3)$ and $\xi = R_{\text{Hill}}/R_{\text{XUV}}$. For the flux, we follow Ribas et al. (2005)

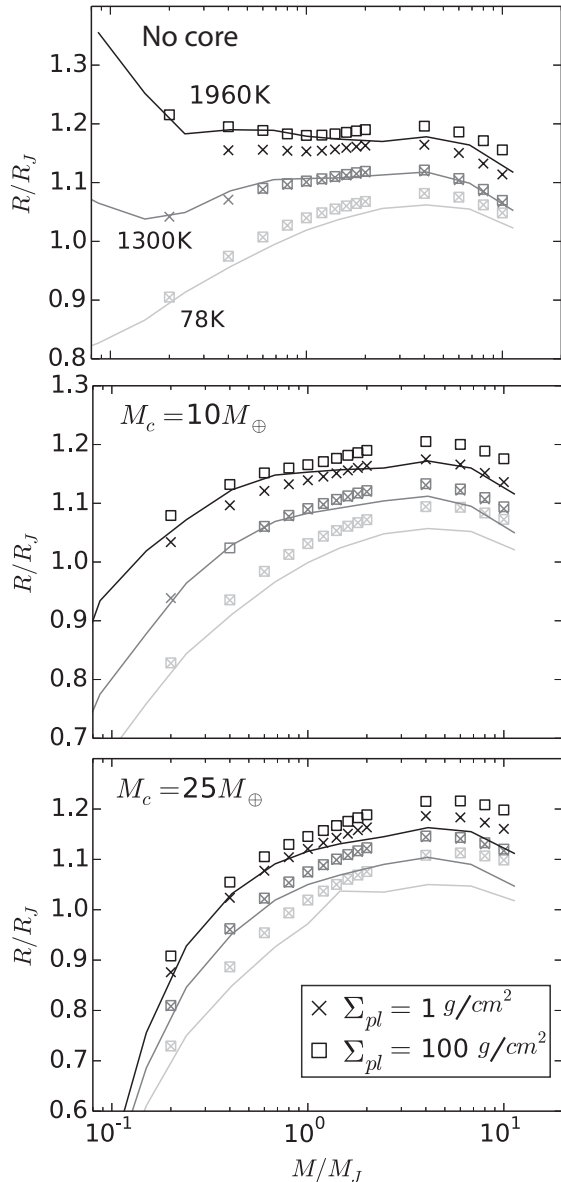


Figure 1. Planetary mass-radius relations at 4.5 Gyr for different core masses and equilibrium temperatures. From top to bottom: core-less planets, $M_c = 10 M_\oplus$, and $25 M_\oplus$, as illustrative examples. The solid lines are the models by Fortney et al. (2007) (from Table 4 of their paper) at an equilibrium temperature of 78 K (light grey), 1300 K (dark grey), and 1960 K (black). The data points are the models computed with MESA for Σ_{pl} set to 1 g/cm^2 (“x”) and 100 g/cm^2 (“□”). Varying Σ_{pl} between $0.1\text{--}1 \text{ g/cm}^2$ makes no significant difference. The value of Σ_{pl} is not important for $T_{\text{eq}} \leq 1300 \text{ K}$ (symbols overlap). As in Fortney et al. (2007), the radii correspond to a pressure of $\sim 1 \text{ bar}$.

and take

$$F_{\text{XUV}} = 29.7 \left(\frac{t}{\text{Gyr}} \right)^{-1.23} \left(\frac{a}{\text{AU}} \right)^{-2} \text{ erg s}^{-1} \text{ cm}^{-2}, \quad (5)$$

where we have scaled their result at 1 AU to an arbitrary distance. The parameter ϵ represents the efficiency of converting F_{XUV} into usable work, while R_{XUV} is the radius of the planet at which the atmosphere becomes optically thick to XUV photons. Murray-Clay et al. (2009) place R_{XUV} at a surface pressure of $\sim 10^{-9} \text{ bar}$, which corresponds to a radius that is typically 10%–20%

greater than the optical photosphere (Lopez & Fortney 2013, hereafter LF13). Here we closely follow the recent results of LF13 and adopt $\epsilon = 0.1$. We note, however, that hydrodynamic calculations suggest that ϵ can vary between 0.01–0.2, depending on the mass of the planet (Owen & Jackson 2012). With $\epsilon = 0.1$, the R_{XUV} value that better matches the results of detailed numerical calculations by LF13 for systems 1–10 Gyr old is $R_{\text{XUV}} = 1.2 R_{\text{pl}}$ (see below) and we use this estimate of R_{XUV} throughout our calculations⁶. Finally, K_{tide} is to account for the fact that the mass leaving the planet needs only to reach the Hill radius to escape, where $R_{\text{Hill}} = M_{\text{pl}}^{1/3} (3M_*)^{-1/3} a$ (Erkaev et al. 2007).

We test the implementation of photo-evaporation by comparing with the mass loss calculations presented by LF13 for the planet Kepler-36c. These are shown in Figure 2. Following their work, we create a $9.4 M_\oplus$, 10 Myr old irradiated planet with a core of $7.4 M_\oplus$ and $Z = 0.35$. We adopt $T_{\text{eq}} = 930 \text{ K}$ (Carter et al. 2012 reports $T_{\text{eq}} = 928 \pm 10 \text{ K}$) and evolve the planetary model with irradiation (fixed) and photo-evaporation, according to Equation (4). The parameters adopted in this work are those yielding agreement with LF13 within a few percent for 1–10 Gyr old systems (black solid line).

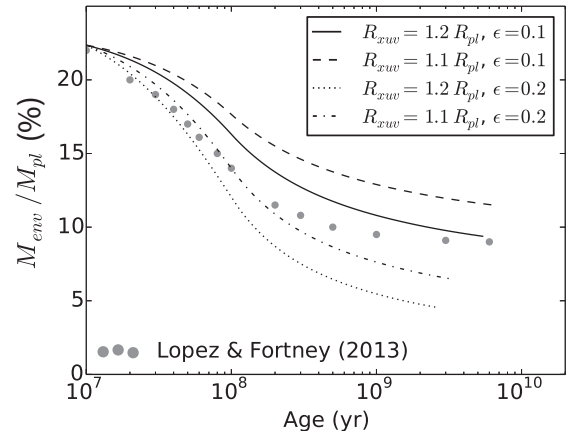


Figure 2. Mass loss evolution of Kepler-36c. Percent of mass contained in the envelope as a function of time for different R_{XUV} and ϵ values. The grey data points are taken from Figure 1 of LF13. The parameter Σ_{pl} was set to 1 g/cm^2 . For F_{XUV} , we follow Ribas et al. (2005), but rescale the flux at the Kepler-36c orbital separation ($a = 0.12 \text{ AU}$). As in LF13, we keep F_{XUV} constant at the 100 Myr value when the star is younger than 100 Myr and we let it evolve when the star is older than 100 Myr. Here we assume a $1 M_\odot$ companion. At the surface ($\tau = 2/3$), the pressure is $\sim 10 \text{ mbar}$ (where LF13 place the transiting radius).

3. ORBITAL EVOLUTION MODEL

MESA allows us to track the evolution of both the planet and star simultaneously, while orbital evolution is followed by taking into account changes to the orbital angular momentum of the system. Below we describe the physical mechanisms included in our model: photo-evaporation (‘PE’), tides, magnetic braking (‘MB’; Skumanich 1972), and RLO. For simplicity, we neglect

⁶ MESA uses automatic mesh refinement, thus adjusting the number of mesh points of the planetary model at the beginning of each timestep, if necessary. For this reason, the point at the surface where the pressure is $\sim 10^{-9} \text{ bar}$ is not always resolved.

the effects of stellar wind mass loss. From the wind prescription provided in MESA’s test suite *1M_{pre-ms.to.wd}* for the evolution of a 1M_⊙ star (Bloeker 1995; Reimers 1975), we find that the orbital evolution timescales associated with stellar winds are longer than 10¹² yr throughout the main-sequence evolution of the host star.

3.1. Photo-Evaporation

Mass escape via photo-evaporation affects the orbital separation and the spin of the planet. For simplicity, we assume spherically symmetric mass loss, which carries away the specific angular momentum of the mass losing component. With this assumption, photo-evaporation affects the orbital angular momentum J_{orb} according to

$$\left(\frac{\dot{J}_{\text{orb}}}{J_{\text{orb}}}\right)_{PE} = \frac{\dot{M}_{\text{pl,PE}}}{M_{\text{pl}}} \frac{1}{1+q} \simeq \frac{\dot{M}_{\text{pl,PE}}}{M_{\text{pl}}}, \quad (6)$$

where $q = M_{\text{pl}}/M_*$. Photo-evaporation is always active and $\dot{M}_{\text{pl,PE}}$ is given by either Equation (3) or Equation (4), depending on F_{XUV} . As far as the planetary spin is concerned, photo-evaporation carries away the angular momentum of the corresponding shells of material.

While we assume that mass loss is spherically symmetric, we note that strong magnetic fields may confine the flow primarily to the poles and day-side of the planet (Owen & Adams 2014). Teyssandier et al. (2015) studied the torque on super-Earth and sub-Neptune-type planets due to anisotropic photo-evaporative mass loss using steady-state one-dimensional wind models. They found that only in rare cases is the planet’s orbit affected by wind torques.

3.2. Tides

Tides affect the stellar and planetary spins, as well as the orbital separation, transferring angular momentum between the orbit and the components’ spin. Within MESA, tides are first applied to the spins. The orbital separation is then varied so as to conserve total angular momentum. Here we take the components to be rotating as solid bodies (however, see Stevenson 1979; Barker et al. 2014).

For *stellar tides* we proceed as in Valsecchi et al. (2014) and Valsecchi & Rasio (2014a,b). Specifically, we adopt the weak-friction approximation (Zahn 1977, 1989) using a parametrization for tidal dissipation calibrated from observations of stellar binaries, as in Hurley et al. (2002). This assumes that tides are dissipated in the stellar convection zone via eddy viscosity. Furthermore, we reduce the efficiency of tides at high tidal forcing frequencies (when the forcing frequency is higher than the convective turnover frequency of the largest eddies) linearly, following Zahn (1966), and as suggested by recent numerical results by Penev et al. (2007).

For *planetary tides*, we assume they efficiently maintain the planet tidally locked ($\Omega_{\text{pl}} = \Omega_{\text{o}}$) throughout the evolution. In fact, for a tidal quality factor $Q' = 10^6$ (typical for gas giants) and a nearly synchronized planet⁷, the spin synchronization timescale due to static

⁷ To get a sense of the magnitude of the spin synchronization timescale we use Equation (10) in Matsumura et al. (2010) and $\Omega_{\text{pl}}(t) = \Omega_{\text{o}}(t - \Delta t)$, where Δt is the distance between two consecutive time steps during an orbital evolution calculation.

tides in the planet is $\sim 2-4$ orders of magnitude shorter than the timescale related to the main driver of the orbital evolution (i.e., mass loss from the planet; see Section 4), depending on the core mass. Clearly, tides would synchronize the planet even faster for lower values of Q' more appropriate for rocky planets. We further discuss tidal locking for the planet in Section 5.

Even though our calculations account for tides in both components, our results show that only stellar tides can affect the orbital separation significantly. In particular, for a slowly spinning stellar host, tides transfer angular momentum from the orbit to the stellar spin, causing orbital decay.

3.3. Magnetic Braking

For the loss of stellar spin angular momentum via magnetic braking we follow Skumanich (1972) and adopt

$$(\dot{\Omega}_*)_{MB} = -\alpha_{MB}\Omega_*^3, \quad (7)$$

where $\alpha_{MB} = 1.5 \times 10^{-14}$ yr (e.g., Barker & Ogilvie 2009; Dobbs-Dixon et al. 2004; Matsumura et al. 2010; Valsecchi & Rasio 2014a,b). This law is well established for the stellar equatorial rotation rates of interest here (1-30 km s⁻¹).

3.4. Roche-Lobe Overflow

RLO is modeled by implicitly computing the mass transfer rate required for the planetary radius to remain below its Roche lobe radius, for which we use the approximation by Eggleton (1983). Here we consider both conservative and non-conservative MT. When MT is conservative, all mass leaving the planet via RLO is accreted onto the star and $\dot{M}_* = -\dot{M}_{\text{pl,RLO}}$. Instead, during non-conservative MT evolution, some fraction δ of $\dot{M}_{\text{pl,RLO}}$ is lost from the system and $\dot{M}_* = -(1 - \delta)\dot{M}_{\text{pl,RLO}}$. Note that in none of the examples presented here does the *star* fill its Roche-lobe during the orbital evolution calculation.

3.4.1. Stable Conservative Mass Transfer

During conservative MT, the evolution of J_{orb} is generally computed under the assumption that MT proceeds through an accretion disk. In the standard picture (e.g., Soberman et al. 1997), the viscosity of the mass flowing through the inner Lagrangian point leads to the formation of a disk around the accretor (Frank et al. 1985). This disk transports mass toward the accretor and angular momentum away from it. The latter is eventually returned to the orbit due to torques operating between the donor and the outer edge of the disk (Lin & Papaloizou 1979) and a small residual angular momentum is transferred to the spin of the star. Our calculations with MESA include spin-up through accretion. However, as the material accreted by the star is only a tiny fraction of its total mass, spin-up due to accretion is negligible.

3.4.2. Stable Non-Conservative Mass Transfer

During non-conservative MT, changes in J_{orb} are computed as in Soberman et al. (1997)

$$\left(\frac{\dot{J}_{\text{orb}}}{J_{\text{orb}}}\right)_{RLO} = \delta\gamma(1+q)\frac{\dot{M}_{\text{pl,RLO}}}{M_{\text{pl}}} \simeq \delta\gamma\frac{\dot{M}_{\text{pl,RLO}}}{M_{\text{pl}}}. \quad (8)$$

This model assumes that a fraction δ of $\dot{M}_{\text{pl,RLO}}$ settles into a ring whose radius a_r is a constant multiple γ^2 of the orbital separation a . This mass is then lost from the system, taking with it the specific angular momentum of the ring. The remaining fraction of the mass $(1 - \delta)$ is assumed to be accreted onto the host star. Below we describe our choices for γ and δ , based on the expected stability of MT.

3.4.3. Considerations on the Stability of Mass Transfer

The calculations presented in Section 4 show that conservative MT is always stable. Instead, some care must be taken when considering non-conservative MT.

For the systems under consideration, the stability of the MT phase depends mainly on the fraction of planetary mass leaving the system, its specific angular momentum, and the response of the planet to mass loss. For a mass-losing planet the latter cannot be determined a priori and it is computed with MESA as the orbital evolution proceeds. As a result, we have no prior knowledge of the values of γ and δ (the parameters regulating the amount of mass leaving the system and how much specific angular momentum is carried away) corresponding to dynamical stability of MT. However, some guidance on the region of stability can be gained as follows. For systems with extreme mass ratios ($q \ll 1$, such as those considered here) and $\dot{J}_{\text{orb}}/J_{\text{orb}}$ given by Equations (6) and (8), the planetary mass during RLO changes according to (e.g., Rappaport et al. 1982 for a derivation)

$$\frac{|\dot{M}_{\text{pl,RLO}}|}{M_{\text{pl}}} \simeq \frac{-2 \left(\frac{\dot{J}_{\text{orb}}}{J_{\text{orb}}} \right)_{\text{tides}} + \left(\frac{\dot{R}_{\text{pl}}}{R_{\text{pl}}} \right)_{\text{therm}} - \frac{\dot{M}_{\text{pl,PE}}}{M_{\text{pl}}} \left(\frac{1}{3} - \xi \right)}{\xi - 2\delta\gamma + \frac{5}{3}}. \quad (9)$$

Here $\xi = (d \ln R_{\text{pl}} / d \ln M_{\text{pl}})_{\text{ad}}$ is the adiabatic logarithmic derivative of radius with respect to mass, $(\dot{R}_{\text{pl}}/R_{\text{pl}})_{\text{therm}}$ is the fractional rate of change of the planet radius due to its thermal evolution, and $(\dot{J}_{\text{orb}}/J_{\text{orb}})_{\text{tides}}$ is the fractional rate of change in orbital angular momentum due to tides. A necessary condition for stable MT is that the denominator of Equation (9) be positive.

Our goal here is to improve on the *stable* MT calculations presented in Valsecchi et al. (2014) by investigating the importance of irradiation effects and self-consistent models for the planet. Therefore, we set $\delta = 1$ and consider γ values for which the MT is expected to be dynamically stable. We discuss possible realistic configurations in Section 5, while reserving a more detailed analysis of MT stability in hot-Jupiter systems to a future study. Such analysis should account for a broad range of γ and δ values, as well as initial orbital configurations and properties of the components (e.g., M_* , M_{pl} , and metallicity; see Section 6).

Without any loss of generality in using Equation (9) we take $\delta = 1$ and $\gamma \neq 0$ and thereby assume that all RLO material leaves the system carrying away a specific angular momentum equal to $\gamma\sqrt{GM_*a}$. The condition for stability then reduces to

$$\gamma < \frac{5}{6} + \frac{\xi}{2}. \quad (10)$$

Equation (10) shows that an increase in the planetary radius with adiabatic mass loss (i.e., $\xi < 0$) has a destabilizing effect, as expected. We test different values of γ with MESA and find that, depending on M_c , the computation becomes numerically difficult for γ values higher than about 0.6 – 0.8. This suggests that the MT may indeed become dynamically unstable and that, according to the criterion in Equation (10), ξ is inferred to be close to zero. To avoid the instability region, while still considering somewhat significant angular momentum loss from the system, we provide examples for non-conservative MT with $\gamma = 0.5$ and $\gamma = 0.6$ for the $1 M_{\oplus}$ and $5 M_{\oplus}$ core cases, respectively, and $\gamma = 0.7$ for the higher core masses.

4. RESULTS

We consider a typical hot-Jupiter system comprising a $1 M_{\odot}$ star and a $1 M_J$ planet at solar metallicity. For the planet we consider $M_c = 1 M_{\oplus}, 5 M_{\oplus}, 10 M_{\oplus}, 15 M_{\oplus}$ and, $30 M_{\oplus}$. The initial period was set to $P_{\text{orb}} = 0.7$ d in all cases. This corresponds to the orbital period at which a hot Jupiter with a $1.5 R_J$ radius would be at its Roche limit and it is chosen arbitrarily to have all systems starting with the same initial period “close enough” to the Roche limit.

For the initial systems’ age we chose 2 Gyr ($t \simeq 20\% t_{\text{MS}}$), as it is at the low end of the ages of the currently known hot Jupiters closest to their Roche-limit separation (see Table 2 in Valsecchi & Rasio 2014a and references therein; see also Section 5). Accordingly, we create 2 Gyr old stellar and planetary models with MESA’s “single-star” module. Each planet is irradiated according to the host star properties at 2 Gyr and the 0.7 d period ($F_* = 5.4 \times 10^9 \text{ erg cm}^{-2} \text{ s}^{-1}$).

The models are then used in MESA’s “binary” module to compute the orbital evolution. During this step both stellar and planetary evolution, as well as irradiation and photo-evaporation are computed self-consistently (Section 2). For the stellar spin, we choose an initial value of $\Omega_* \sim 0.1 \Omega_{\odot}$. This is consistent with the observed slow stellar rotation rates for the tightest hot-Jupiter systems known ($\Omega_* \simeq 0.1 - 0.2 \Omega_{\odot}$; see Table 1 in Valsecchi & Rasio 2014a). We take the planet to be tidally locked throughout the evolution (see Section 5 for a discussion). Finally, as described in Section 3.4, we consider both conservative and non-conservative MT.

The results are presented as follows. In Section 4.1 we describe qualitatively how P_{orb} evolves as the planet loses mass, for different values of M_c . In Section 4.2 we describe in detail the evolution of the $5 M_{\oplus}$ and $30 M_{\oplus}$ core cases. We take these as extreme examples among those considered here. In fact, as described below (Section 4.1), the behavior of the $1 M_{\oplus}$ core model needs a more in-depth investigation. For $M_c = 5 M_{\oplus}$ and $M_c = 30 M_{\oplus}$, we mainly focus on the non-conservative MT evolution and briefly describe the conservative case at the end of each section. For these same core masses, we also investigate the effect of varying the column density for irradiation in Section 4.2.3. A summary of the results for all core masses and physical assumptions is presented in Table 2.

Here we note that some of the evolutionary calculations described below become numerically challenging when little mass is left in the envelope ($M_{\text{env}}/M_{\text{pl}} \lesssim$

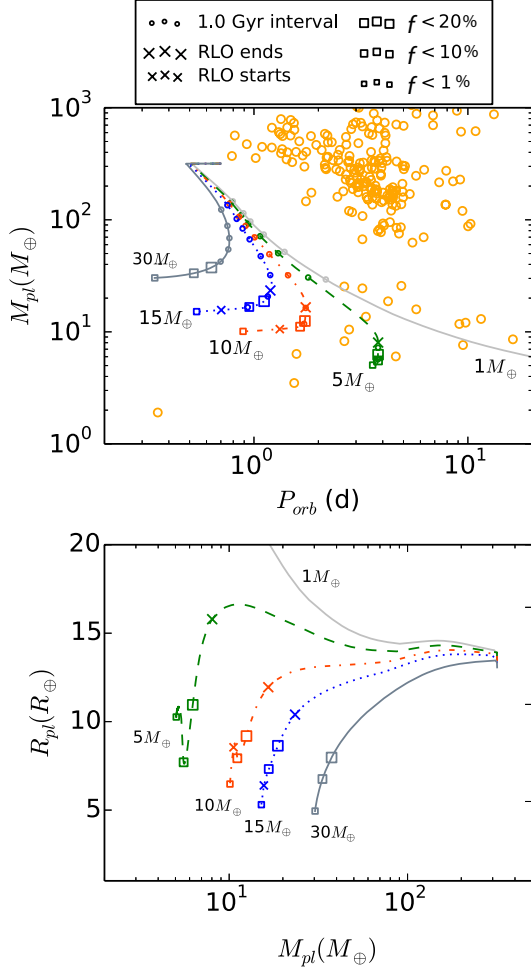


Figure 3. Planetary mass as a function of the orbital period (top) and mass-radius relation (bottom) for conservative MT (with $\delta = 0$). The open orange circles are confirmed exoplanetary systems (NASA Exoplanet Archive, 13 January 2015) with observationally inferred M_{pl} and P_{orb} , and hosting one planet only, for simplicity. The colored lines are our evolutionary models for different core masses. Evolution in time proceeds downward. For the various symbols: “x” mark the end/start of RLO, “□” mark times when the mass in the envelope drops below $f = 20\%$, 10% , and 1% of the total mass. The colored open circles along each evolutionary track in the top panel mark 1 Gyr intervals.

1%). Therefore, we show the evolution up to when $M_{\text{env}}/M_{\text{pl}}$ drops just below 1%. Prior to this time, we encounter convergence problems for the $5 M_{\oplus}$ and $10 M_{\oplus}$ core models during non-conservative MT (when $M_{\text{env}}/M_{\text{pl}} \leq 1.9\%$ for the former and $M_{\text{env}}/M_{\text{pl}} \leq 2.6\%$ for the latter). In any case, in all examples considered the evolution is quite rapid after the planet is left with only a few percent of the envelope mass. Thus, we discuss it qualitatively, guided by the relevant timescales entering the problem.

4.1. The General Behavior

Evolutionary examples for conservative and non-conservative MT are shown in Figures 3 and 4, respectively. The top panels show the evolution of the orbital period with the planet’s mass. For comparison, the positions of the observed planets are the orange open circles. The bottom panels show the corresponding evolutionary tracks for planetary mass and radius. The different core

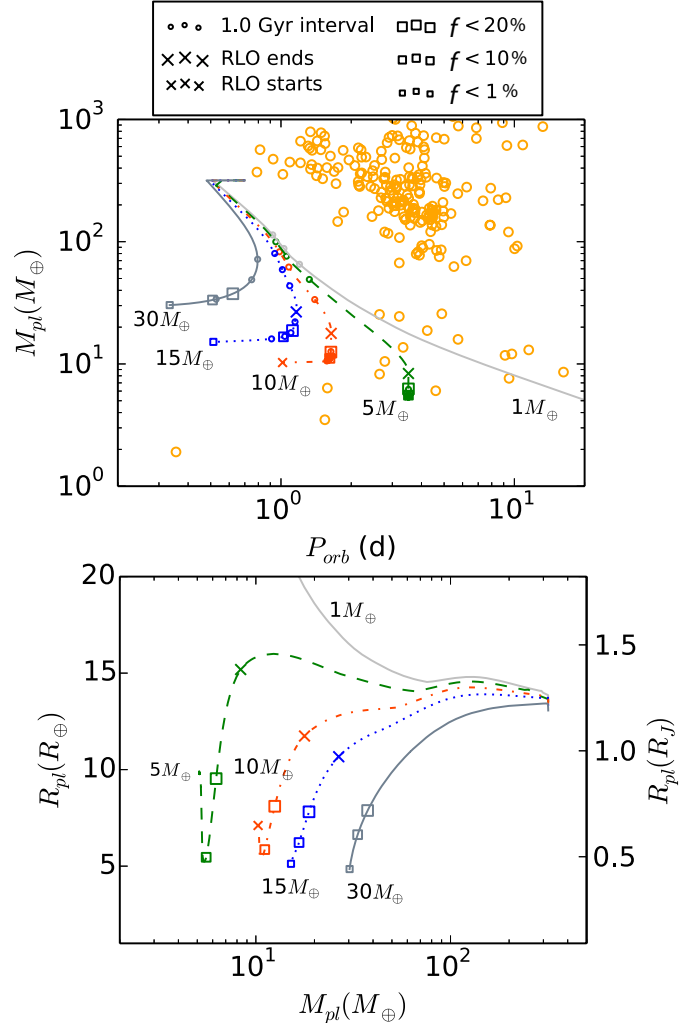


Figure 4. Same as Figure 3 but for non-conservative MT (with $\delta = 1$). We use $\gamma = 0.5, 0.6$, and 0.7 for $M_c = 1 M_{\oplus}, 5 M_{\oplus}$, and $\geq 10 M_{\oplus}$, respectively. Note, for the $5 M_{\oplus}$ and $10 M_{\oplus}$ core models the evolution terminates because of convergence problems when the envelope contains $\simeq 1.9\%$ and $\simeq 2.6\%$ of the total mass, respectively. For the $5 M_{\oplus}$ core model described in detail in the text, the various symbols in the top panel are all superimposed at the end of the evolution, where the planet spends few Gyrs.

masses are denoted with different colors and line-styles. For all cases considered, the MT proceeds on a timescale longer than the thermal timescale of the planet. Thus, the planet remains in thermal equilibrium throughout the MT. Here we note that our $1 M_{\oplus}$ core model shows a severe increase in R_{pl} that needs further investigation. In fact, R_{pl} increases up to about $10 R_J$ when $M_{\text{pl}} \simeq 1 M_{\oplus}$. However, we note also that the core-less models in Figure 8 of Fortney et al. (2007) have radii ranging between $R_{\text{pl}} \simeq 0.8 - 2.3 R_J$ when $M_{\text{pl}} \sim 30 M_{\oplus}$ (the lowest mass considered by Fortney et al. 2007 for a core-less Jupiter), depending on the age of the planet and the level of irradiation. This range encompasses our radii for masses down to $\sim 10 M_{\oplus}$. We omit the $1 M_{\oplus}$ core model from the subsequent discussion.

The evolution in time in the $M_{\text{pl}} - P_{\text{orb}}$ ($R_{\text{pl}} - M_{\text{pl}}$) diagram proceeds downward (right to left). The shape of the evolutionary tracks in such diagram depends on the competing effects of stellar tides (tending to shrink

the orbit) and RLO (tending to expand the orbit). The $R_{\text{pl}} - M_{\text{pl}}$ tracks in the bottom panels of Figures 3 and 4 partly determine which mechanism dominates. In fact, in addition to tides, RLO affects the orbital separation according to

$$\frac{\dot{a}_{\text{RLO}}}{a} \sim 2 \frac{\dot{M}_{\text{pl,RLO}}}{M_{\text{pl}}} (\delta\gamma - 1) > 0 \quad (11)$$

[Equation (8)], and $|\dot{M}_{\text{pl,RLO}}/M_{\text{pl}}|$ is partly determined by the response of the planetary radius to mass loss.

At the onset of RLO, the nearly constant or increasing R_{pl} with decreasing M_{pl} (in particular, if $\xi < 1/3$) causes the RLO term to dominate over the tidal contribution. As a result the orbit expands. This behavior persists until the mass-radius relation begins steepening, becoming more positive. At this point, the tidal term becomes more significant than the RLO term and the orbit begins to shrink. In some cases ($M_{\text{c}} = 5 M_{\oplus}, 10 M_{\oplus}, 15 M_{\oplus}$), the combination of the planet shrinking in response to mass loss and the weakening tidal forces with decreasing M_{p} causes the RLO phase to stop and the planet to detach (bigger “×” symbols). In few cases ($M_{\text{c}} = 10 M_{\oplus}, 15 M_{\oplus}$), as the star approaches the end of its main sequence, the tidally-driven orbital shrinkage and the irradiation-driven increase in R_{pl} (e.g., Fortney & Nettelmann 2010) lead to a second RLO phase (smaller “×” symbols, denoted with $t_{\text{RLO},2}$ in Table 2). Note that none of the observed exoplanets in Figures 3 and 4 is currently in RLO. Therefore, observations should be compared with the portion of the evolutionary tracks where the planet is detached.

Finally, we note that the shape of the evolutionary tracks does not change significantly in the $M_{\text{pl}} - P_{\text{orb}}$ diagram between conservative and non-conservative MT. However, as summarized in Table 2 and described in the following sections, whether mass is lost from the system does affect the duration of the various phases mentioned above.

4.2. Detailed Examples: Different Core Masses

4.2.1. The $5 M_{\oplus}$ Core Model

Figure 5 shows the evolution of a Jupiter with a $5 M_{\oplus}$ core undergoing non-conservative MT. For the first ~ 80 Myr the orbit shrinks, as tides transfer angular momentum from the orbit to the stellar spin, trying to spin-up the star. Eventually, when $P_{\text{orb}} \simeq 0.5$ d ($a \simeq 0.01$ AU) the planet fills its Roche-lobe.

At the onset of RLO, the response of the radius to mass loss causes the orbit to expand [Equation (11)]. During this phase, mass is removed from the planet at a rate varying between $\sim 10^{-14} - 10^{-12} M_{\odot} \text{ yr}^{-1}$ ($10^{12} - 10^{14} \text{ g s}^{-1}$). When the system is about 5.8 Gyr old and the planet has lost $\sim 97\%$ of its mass (and $M_{\text{pl}} \simeq 8.4 M_{\oplus}$), the planetary mass-radius relation begins steepening and RLO stops. This event is marked with a “×” in Figure 4. At this stage, $P_{\text{orb}} \simeq 3.5$ d ($a \simeq 0.04$ AU).

The post-RLO phase is driven mainly by photo-evaporation. In fact, the tidal decay timescale is longer than a Hubble time for the majority of this phase. Photo-evaporation removes mass from the planet at a rate of $\sim 10^{-15} M_{\odot} \text{ yr}^{-1}$ (10^{11} g s^{-1}) and it does not affect the

orbital separation significantly. For about 4 Gyr (until the system is about 9.5 Gyr old) the planet remains in a 3.5 d orbit and its mass decreases from about $8.4 M_{\oplus}$ to about $5.4 M_{\oplus}$ (when $M_{\text{env}}/M_{\text{pl}} \simeq 7.4\%$). Eventually, the star approaches the end of its main sequence lifetime and it begins expanding. The increase in R_{\star} causes a decrease in the tidal timescales and an increase in the amount of irradiation received by the planet. The latter occurs because R_{\star} evolves faster than T_{\star} in Equation (1). Such increase in irradiation yields an increase in R_{pl} and, as a consequence, stronger photo-evaporation. The rate of mass loss from the planet increases by about an order of magnitude ($\sim 10^{-14} M_{\odot} \text{ yr}^{-1} = 10^{12} \text{ g s}^{-1}$). At the end of the calculation, we are left with a $\simeq 5.1 M_{\oplus}$ planet ($M_{\text{env}}/M_{\text{pl}} \simeq 1.9\%$) in a 3.4 d orbit.

The remainder of the evolution depends mainly on the tidal timescale compared with the stellar nuclear evolution timescale. The former determines the rate of tidal decay (leading to a second planetary RLO), while the latter determines the rate of stellar expansion (leading to stellar RLO). Given the (very steep) dependence of the tidal decay timescale on $(a/R_{\star})^8$ (e.g., Valsecchi & Rasio 2014b), we argue that tides will likely drive the planet down to its Roche limit. Here, it will be stripped of the remaining envelope and, assuming a constant density for the core, it will be consumed at approximately constant P_{orb} on the rapid tidal decay timescale. This follows from Paczyński’s (1971) approximation for the Roche limit separation $a_{\text{R}} = (R_{\text{pl}}/0.462)(M_{\star}/M_{\text{pl}})^{1/3} \propto (M_{\star}/\rho_{\text{pl}})^{1/3}$, where ρ denotes the density.

In the case of conservative MT, the orbital evolution proceeds similarly to the examples presented above, but the duration of the various phases is different. This is summarized in Table 2. In particular, the RLO phase lasts until the system is about 9 Gyr old. At this stage the planet has a mass of $M_{\text{pl}} \simeq 8 M_{\oplus}$ and the orbital period is $P_{\text{orb}} \simeq 3.8$ d. The remainder of the evolution proceeds similarly to the non-conservative case. However, the detached evolution has a shorter duration because soon ($\simeq 1$ Gyr) after the end of RLO the star is approaching the end of its MS.

4.2.2. The $30 M_{\oplus}$ Core Model

Figure 6 shows the evolution of a Jupiter with a $30 M_{\oplus}$ core undergoing non-conservative MT. For the first ~ 80 Myr tides cause the orbit to shrink. As for the $5 M_{\oplus}$ core case the planet fills its Roche lobe when $P_{\text{orb}} \simeq 0.5$ d. At the onset of RLO, the orbit expands as mass is removed from the planet at a rate of $\sim 10^{-13} M_{\odot} \text{ yr}^{-1}$ (10^{13} g s^{-1}). As tides act on a timescale of ~ 1 Gyr for this higher core mass, the orbit begins shrinking about 1 Gyr after the beginning of RLO. The RLO phase continues until the system is about 5.2 Gyr old, when $M_{\text{env}}/M_{\text{pl}} \leq 1\%$ and we interrupt the calculation. At this time, $M_{\text{pl}} = 30.3 M_{\oplus}$ and $P_{\text{orb}} = 0.3$ d.

The difference with the $5 M_{\oplus}$ core model described in Section 4.2.1 lies in the earlier (at higher M_{pl} ; Figure 4) decrease in planetary radius. This behavior of the radius for decreasing mass yields a less severe mass loss during RLO and a consequent less dramatic orbital expansion. As a result, the orbital evolution proceeds at shorter orbital periods and the planet never shrinks back inside its

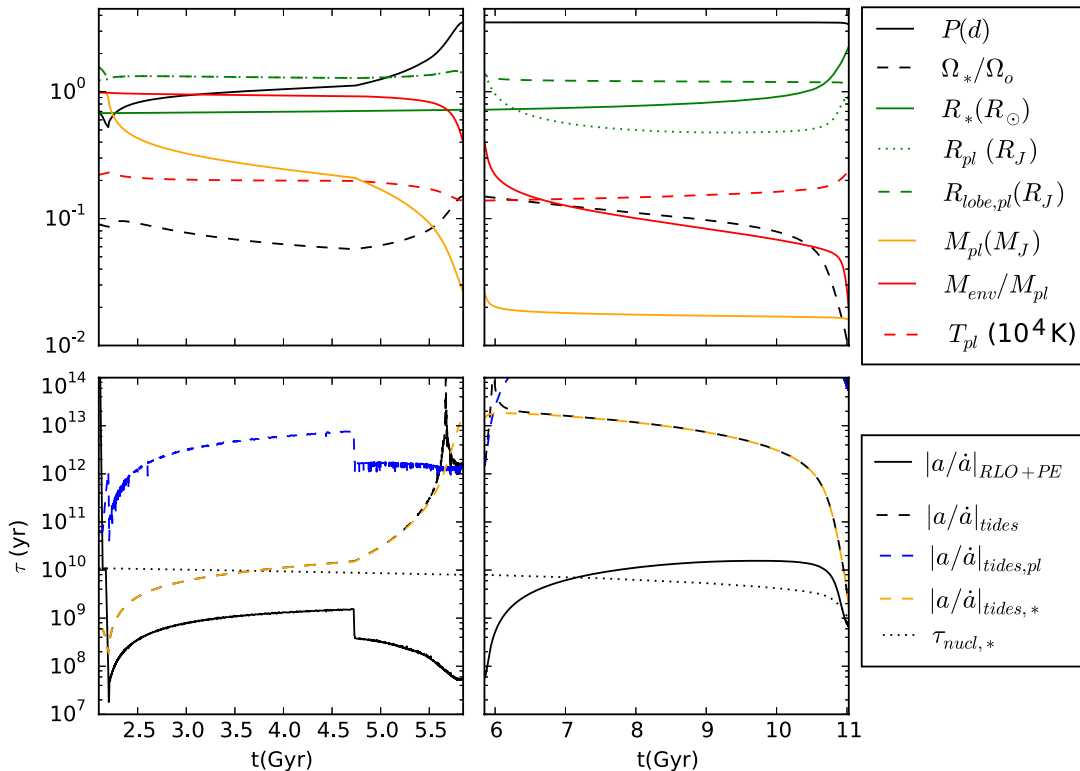


Figure 5. Detailed evolution of some of the components and orbital parameters (top) and of the relevant timescales (bottom) for a Jupiter with $M_c = 5 M_\oplus$. For this evolution we adopt the parameters $\delta = 1$ and $\gamma = 0.6$. The subscripts “RLO+PE”, “tides”, and “nucl” refer to the timescales associated with mass changes due to Roche-lobe overflow and photo-evaporation, tides, and the star’s nuclear timescale, respectively. For tides we show the stellar and planetary contribution in orange and blue, respectively, but note that only stellar tides play a significant role, as the planetary tides timescale is always longer than a Hubble time. On the left is the evolution during the RLO phase. Here, the green dotted and dashed lines, representing R_{pl} and $R_{lobe,pl}$, respectively, overlap. On the right is the evolution when the planet goes back within its Roche-lobe, and $R_{pl} < R_{lobe,pl}$. The sudden decrease in $|a/\dot{a}|_{RLO+PE}$ at $\simeq 4.7$ Gyr (bottom-left panel) occurs when mass loss via photo-evaporation transitions from “radiation/recombination” limited [Equation (3)] to “energy” limited [Equation (4)].

Roche-lobe.

Even though our results show the evolution until $M_{env}/M_{pl} \leq 1\%$, the relevant timescales suggest that the orbit will shrink until the envelope is completely removed. Subsequently, if the core has a constant density, it will be consumed at constant orbital period on the rapid (≤ 100 Myr, at the end of the evolution in Figure 6) tidal decay timescale.

As for the $5 M_\oplus$ core model, the evolution during conservative MT varies only insofar as the duration of the RLO phase is concerned (see Table 2). In fact, during conservative MT the evolution lasts until the system is about 7.8 Gyr old and the planet never stops RLO. At the end of the calculation (when $M_{env}/M_{pl} \simeq 1\%$) $P_{orb} = 0.3$ d.

4.2.3. Varying the Column Density for Irradiation

For highly irradiated planets with $M_{pl} < M_J$, the mass-radius relations of Fortney et al. (2007) in Figure 1 are bracketed by those computed with MESA for $\Sigma_{pl} = (1-100) \text{ g/cm}^2$. We test the effect of increasing Σ_{pl} by two orders of magnitude in the $5 M_\oplus$ and $30 M_\oplus$ core mass models. We find that the overall evolution does not change significantly (see Table 2). Qualitatively, R_{pl} is a few percent larger. As a result, for the same evolutionary time, RLO starts and proceeds at a longer orbital period. For the $5 M_\oplus$ core model, the orbital period is a few percent longer than in the smaller Σ_{pl} case. For the

$30 M_\oplus$ core model, the percent difference in orbital period increases ($\sim 1\%$ at the beginning of RLO to $\sim 10\%$ at the end) as the evolution proceeds. As a result, mass loss proceeds on a longer timescale. Consequently, for the same evolutionary time, the models with higher Σ_{pl} retain a larger fraction of the envelope. This yields a longer duration of the RLO phase and a longer orbital period at the end of RLO.

5. DISCUSSION

The stable MT calculations presented here show that the more non-conservative is the MT, the shorter is the duration of the RLO phase. In turn, the duration of the detached phase is correspondingly longer. In particular we find that a hot Jupiter going through a phase of non-conservative MT detaches when its envelope contains tens of per cent of the total mass (i.e., Figures 3, 4, and 5). After RLO has ended the planet spends a few Gyr losing the remainder of its envelope via photo-evaporation at nearly constant orbital period. For example, a Jupiter with a $5 M_\oplus$ core (Section 4), remains detached for a few Gyrs at an orbital period of 3.5 d. During this time its envelope mass fraction drops from $\sim 20\%$ when the system is about 6 Gyr to about 2% when the star approaches the end of its main sequence lifetime. A similar evolution occurs for $M_c = 10 M_\oplus$ and $15 M_\oplus$, with an increasingly shorter duration of the detached phase for increasingly massive cores. Interest-

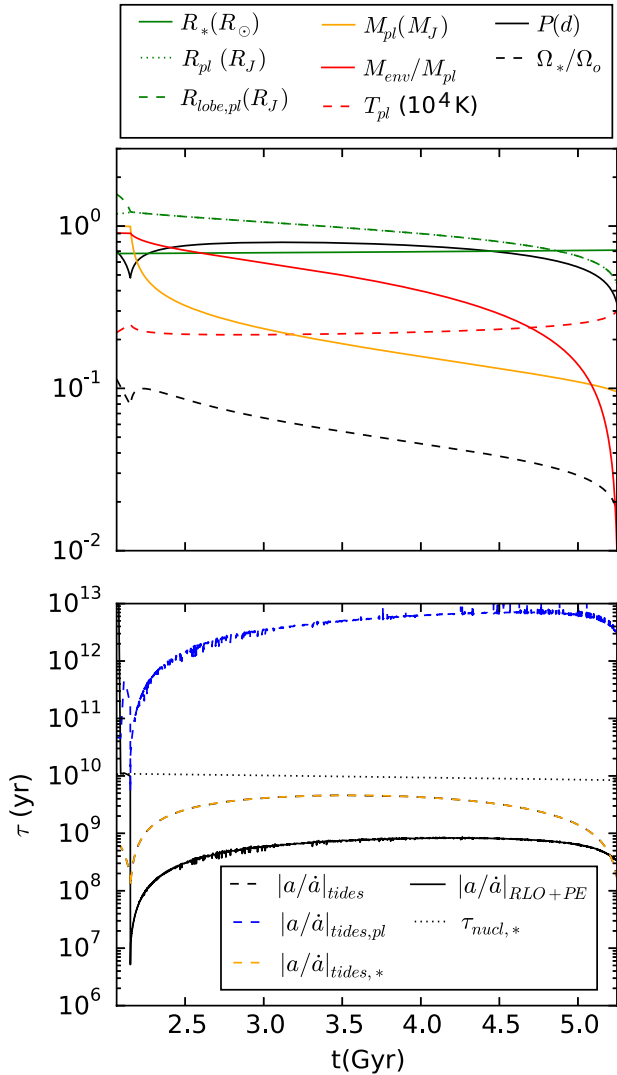


Figure 6. Same as Figure 5 but for a Jupiter with $M_c = 30 M_\oplus$ and $\gamma = 0.7$.

ingly, the bulk density of *known* super-Earth and sub-Neptunes-type planets suggests that many such planets consist of a core (rocky or icy) surrounded by an H/He envelope comprising up to tens of a percent of the total mass (Lopez & Fortney 2014). While this agreement with our MT models is very promising, our calculation neglects some important effects which we discuss below. A discussion of observational signatures is in Section 5.3.

5.1. Mass Transfer Scenarios and Stability

In this work we neglected the effects of magnetic fields and stellar winds on the RLO material. These mechanisms can affect the flow of MT (e.g., Cohen & Glocer 2012; Owen & Adams 2014), potentially playing a crucial role in determining whether any mass is transferred or an accretion disk ever forms. On the opposite side of conservative MT, is the case where mass is blown away directly from the planet or the inner Lagrangian point (L_1). For a $1M_J$ planet and a $1M_\odot$ star, L_1 is located at $\simeq 0.93a$ [Lai et al. 2010; Equation (10)]. In the formalism of Section 3 these scenarios can be reproduced by setting $\delta = 1$ and $\gamma = 1$ (mass lost from the planet) or $\gamma = 0.97$ (mass loss from L_1). In this configuration,

Equation (10) requires ξ to be larger than (0.27-0.33) in order for the MT to be dynamically stable. We perform test runs with MESA fixing $\delta = 1$ while varying γ . We find that the MT may become dynamically unstable for $\gamma \geq 0.8$. In fact, the computation becomes numerically difficult, with the integrator time-step dropping to less than one month. This limit on γ for stability suggests that the effective value of ξ is close to zero (as directly computed within MESA).

Alternatively, one may consider the case where matter flows in a narrow stream from the L_1 point, attempting to form a ring around the star which is then blown away. This case has been discussed in the context of MT stability in stellar binary systems (e.g., Lubow & Shu 1975; Hut & Paczynski 1984; Verbunt & Rappaport 1988). If, in fact, the ring size is too narrow to tidally interact with the donor, then the angular momentum will not be returned to the orbit. In this case, the angular momentum leaving the system would be determined by how much angular momentum a particle has before it is blown away (i.e. by the mean ring radius r_d). We combine calculations by Hut & Paczynski (1984), covering M_{pl}/M_* down to 10^{-3} , with our own calculations, extending these down to $M_{pl}/M_* = 10^{-6}$. We compute r_d to range between $\simeq 0.7-0.9$ for a $1M_J-10M_\oplus$ planet. This range implies γ values between $\simeq 0.84-0.95$ and a value of ξ for stability between $\simeq 0-0.23$ [Equation (10)]. This scenario appears borderline between stable and unstable MT. Clearly any scenario where $\gamma > 1$ would be dynamically unstable.

If the MT were indeed dynamically unstable, one could envision the system undergoing a common-envelope-like evolution (‘CE’), that is somewhat distinct from the standard binary stellar evolution picture (Webbink 1984). We envision that the envelope of the planet would quickly flow through the inner Lagrange point and form a disk-like structure around the host star. The core of the planet would then find itself orbiting within this ring or disk of envelope material. Depending on the detailed core-disk interactions, the core may spiral-in toward the host star and eject the disk. This is distinct from the usual CE scenario in that the envelope of the planet becomes bound to the host star, rather than the planet, and it is the planet which ejects its own envelope via tidal and viscous interactions. Insights into the outcome of such a phase can then be gained from the energy equation

$$\alpha_{CE} \left[\frac{GM_*M_c}{2a_f} - \frac{GM_*M_{pl}}{2a_i} \right] \simeq \frac{GM_*M_{env}}{2a_i}. \quad (12)$$

Here, α_{CE} represents the efficiency with which the planet core’s orbital energy can be used to unbind the envelope material which is now in a ring around the host star. The parameters a_i and a_f denote the orbital separation at the onset and at the end of this ‘CE’ phase, respectively. Equation (12) can be directly solved for the ratio of a_f/a_i , and we find:

$$\frac{a_f}{a_i} \simeq \frac{\alpha_{CE}M_c}{\alpha_{CE}M_{pl} + M_{env}}. \quad (13)$$

For plausible values of α_{CE} near unity, this expression yields $a_f/a_i \simeq M_c/2M_{pl}$. This, in turn, implies that the orbital separation would decay by a factor of more than an order of magnitude.

Thus, all cores considered in this work would reach their own Roche limit in the event of unstable RLO⁸. A new RLO phase would then begin driven, this time, by the interplay of viscous drag on the core due to the remaining envelope mass orbiting the host, and the back-reaction from stable MT through RLO. The former would tend to shrink the orbit, while the latter would make the orbit expand.

The actual outcome of an unstable MT phase from a hot Jupiter to its stellar host is still an unexplored question which we are currently addressing via smoothed-particle hydrodynamics simulations. Furthermore, magnetohydrodynamics (MHD) simulations are needed to determine the role played by magnetic fields. Here we note that Matsakos et al. (2015) recently investigated magnetized star-planet interactions via 3D MHD numerical simulations including stellar wind and photo-evaporative mass loss. They found that, depending on the planet’s magnetic field and outflow rate, as well as the stellar gravitational field, the star can accrete part of the mass lost by the planet via photo-evaporation. Pillitteri et al. (2015) performed a similar analysis for the specific case of HD 189733.

5.2. Planetary Tides

Here we took planetary tides to be efficient in keeping the spin of the planet tidally locked. This assumption is justified by the magnitude of the tidal synchronization timescales discussed in Section 3. However, we neglected the resulting effects of tidal dissipation on the planetary structure. These include potentially significant heating, inflation, and resulting stronger mass loss. To gain some intuition on their significance we compute the energy deposited between two consecutive integration steps and compare it with the planetary binding energy. For the former we use $\Delta E_{\text{tide}} = \frac{1}{2} I_{\text{pl}} |\Omega_{\text{o}}^2(t + \Delta t) - \Omega_{\text{o}}^2(t)|$, where I_{pl} is the moment of inertia, while for the latter we use $E_{\text{bind}} = \eta GM_{\text{pl}}^2/R_{\text{pl}}$. Assuming a uniform density planet ($\eta = 3/5$), $\Delta E_{\text{tide}}/E_{\text{bind}}$ is between $10^{-3} - 10^{-4}$. A core would increase the central density, thus decreasing ΔE_{tide} even further. This suggests that the energy deposited in the planet via tides may not affect its structure dramatically.

5.3. Observational Signatures

As discussed in Valsecchi et al. (2014), this evolutionary scenario has several observational consequences. First, the properties of stars hosting hot Jupiters and those hosting Super-Earth and mini-Neptunes-type planets should be similar. Furthermore, depending on the core mass and the details of the MT process (whether any mass is lost from the system and where angular momentum is removed from), a system may spend enough time in RLO that it might be possible to observe planets in such a phase. If MT really proceeds through an accretion disk, this may produce observational signatures (e.g., line absorption of stellar radiation and time-dependent obscuration of the starlight; Lai et al. 2010). Finally, the results in Figures 3 and 4, and in Table 2 suggest that,

⁸ If R_* is too large, the planet-core will plunge into its atmosphere before filling its Roche lobe; the critical period for tidal breakup of a rocky body can be $\lesssim 5$ hours (Rappaport et al. 2013).

if this model is a viable formation channel for super-Earth and mini-Neptune-type planets, there should be a correlation between M_{pl} and P_{orb} . Specifically, the more massive planets should be found at shorter orbital periods. This is a major result when compared to the simple model of Valsecchi et al. (2014). In fact, without a self-consistent calculation of planetary evolution and irradiation effects we had found no trend between final $M_{\text{pl}} - P_{\text{orb}}$ pairs. This inverse correlation between orbital period and planetary mass also suggests that dynamically stable MT phases like those presented here do not seem to represent a viable channel for the formation of the so-called ultra-short-period planets (e.g., Sanchis-Ojeda et al. 2014 and reference therein). These planets have typical radii smaller than $2R_{\oplus}$ (corresponding to a mass of about $5M_{\oplus}$; Weiss & Marcy 2014) and orbital periods shorter than one day.

6. CONCLUSIONS

In this paper we presented the first evolutionary calculations of irradiated hot-Jupiters undergoing tidally-driven Roche-lobe overflow (RLO). We found that, depending on the size of the planetary core and the details of the mass transfer, the RLO phase and, in turn, the detached phase (after RLO had ceased) can last from a few to several Gyrs. For the smaller core masses ($M_c \leq 15M_{\oplus}$), after most of the envelope has been removed during RLO, the planet spends a few Gyrs losing mass via photo-evaporation at nearly constant orbital period. This is consistent with the density of known super-Earths and sub-Neptunes, for which detailed modeling (Lopez & Fortney 2014) place tens of percent of the total mass in a H/He envelope surrounding a rocky core.

Here we considered a coarse grid of core masses and *one* initial binary configuration. However, as summarized in Tables 1 and 2 of Valsecchi & Rasio 2014a, the tightest hot-Jupiters systems comprise a variety of stellar and planetary masses ($\simeq 0.87 - 1.33M_{\odot}$ and $\simeq 0.46 - 1.49M_J$), as well as metallicities ($Fe/H \simeq -0.35 - 0.22$) and ages (1.5–13 Gyr). All these parameters may affect the efficiency of tides and, thus, the evolution of a Jupiter undergoing RLO. This variety of properties requires a more refined parameter space in initial component and orbital properties, as well as planetary core masses (especially in the $M_c \leq 15M_{\oplus}$ regime; Figures 3 and 4). Such a parameter space study should also explore in more detail the boundaries for MT stability. Future observations of increasingly massive super-Earths and sub-Neptunes-type planets in increasingly tighter orbits might provide an important observational test of the ideas presented.

Finally, we remark that the value of $\gamma\delta$, the parameter describing mass and specific angular momentum loss, is crucial to the stability of RLO mass transfer. Where matter goes after RLO, and how much of it is actually accreted by the host star or ejected from the system, can only be determined by hydrodynamic calculations. The results of such calculations could well determine whether hot Jupiters can undergo the kind of stable RLO mass transfer described in this work.

FV and FAR are supported by NASA Grant NNX12AI86G. FV is also supported by a CIERA fellowship. LAR gratefully acknowledges support provided by NASA through Hubble Fellowship grant #HF-51313 awarded by the Space Telescope Science Institute, which is operated by the Association of Universities for Research in Astronomy, Inc., for NASA, under contract NAS 5-26555. We thank Dorian Abbot, Arieh Konigl, Titos Matsakos, Ruth Murray-Clay, James Owen, and Dave Stevenson for useful discussions. This work used computing resources at CIERA funded by NSF PHY-1126812. This research has made use of the NASA Exoplanet Archive, which is operated by the California Institute of Technology, under contract with the National Aeronautics and Space Administration under the Exoplanet Exploration Program.

REFERENCES

- Barker, A. J., Dempsey, A. M., & Lithwick, Y. 2014, *ApJ*, 791, 13
- Barker, A. J., & Ogilvie, G. I. 2009, *MNRAS*, 395, 2268
- Batygin, K., & Stevenson, D. J. 2013, *ApJ*, 769, L9
- Birkby, J. L., Cappetta, M., Cruz, P., et al. 2014, *MNRAS*, 440, 1470
- Bloeker, T. 1995, *A&A*, 297, 727
- Carter, J. A., Agol, E., Chaplin, W. J., et al. 2012, *Science*, 337, 556
- Chatterjee, S., Ford, E. B., Matsumura, S., & Rasio, F. A. 2008, *ApJ*, 686, 580
- Cohen, O., & Glocer, A. 2012, *ApJ*, 753, L4
- Damiani, C., & Lanza, A. F. 2014, *ArXiv e-prints*, arXiv:1411.3802
- Dobbs-Dixon, I., Lin, D. N. C., & Mardling, R. A. 2004, *ApJ*, 610, 464
- Eggleton, P. P. 1983, *ApJ*, 268, 368
- Erkaev, N. V., Kulikov, Y. N., Lammer, H., et al. 2007, *A&A*, 472, 329
- Fabrycky, D., & Tremaine, S. 2007, *ApJ*, 669, 1298
- Fortney, J. J., Marley, M. S., & Barnes, J. W. 2007, *ApJ*, 659, 1661
- Fortney, J. J., & Nettelmann, N. 2010, *Space Sci. Rev.*, 152, 423
- Frank, J., King, A. R., & Raine, D. J. 1985, *Accretion power in astrophysics*
- Goldreich, P., & Tremaine, S. 1980, *ApJ*, 241, 425
- Howard, A. W., Sanchis-Ojeda, R., Marcy, G. W., et al. 2013, *Nature*, 503, 381
- Hurley, J. R., Tout, C. A., & Pols, O. R. 2002, *MNRAS*, 329, 897
- Hut, P., & Paczynski, B. 1984, *ApJ*, 284, 675
- Jackson, B., Barnes, R., & Greenberg, R. 2009, *ApJ*, 698, 1357
- Jackson, B., Miller, N., Barnes, R., et al. 2010, *MNRAS*, 407, 910
- Lai, D., Helling, C., & van den Heuvel, E. P. J. 2010, *ApJ*, 721, 923
- Lin, D. N. C., Bodenheimer, P., & Richardson, D. C. 1996, *Nature*, 380, 606
- Lin, D. N. C., & Papaloizou, J. 1979, *MNRAS*, 186, 799
- Lopez, E. D., & Fortney, J. J. 2013, *ApJ*, 776, 2
- , 2014, *ApJ*, 792, 1
- Lopez, E. D., Fortney, J. J., & Miller, N. 2012, *ApJ*, 761, 59
- Lubow, S. H., & Shu, F. H. 1975, *ApJ*, 198, 383
- Matsakos, T., Uribe, A., & Königl, A. 2015, *ArXiv e-prints*, arXiv:1503.03551
- Matsumura, S., Peale, S. J., & Rasio, F. A. 2010, *ApJ*, 725, 1995
- Metzger, B. D., Giannios, D., & Spiegel, D. S. 2012, *MNRAS*, 425, 2778
- Murray, N., Hansen, B., Holman, M., & Tremaine, S. 1998, *Science*, 279, 69
- Murray-Clay, R. A., Chiang, E. I., & Murray, N. 2009, *ApJ*, 693, 23
- Nagasawa, M., Ida, S., & Bessho, T. 2008, *ApJ*, 678, 498
- Naoz, S., Farr, W. M., Lithwick, Y., Rasio, F. A., & Teyssandier, J. 2011, *Nature*, 473, 187
- Owen, J. E., & Adams, F. C. 2014, *MNRAS*, 444, 3761
- Owen, J. E., & Alvarez, M. A. 2015, *ArXiv e-prints*, arXiv:1504.07170
- Owen, J. E., & Jackson, A. P. 2012, *MNRAS*, 425, 2931
- Owen, J. E., & Wu, Y. 2013, *ApJ*, 775, 105
- Paczynski, B. 1971, *ARA&A*, 9, 183
- Paxton, B., Bildsten, L., Dotter, A., et al. 2011, *ApJS*, 192, 3
- Paxton, B., Cantiello, M., Arras, P., et al. 2013, *ApJS*, 208, 4
- Paxton, B., Marchant, P., Schwab, J., et al. 2015, *ArXiv e-prints*, arXiv:1506.03146
- Penev, K., Sasselov, D., Robinson, F., & Demarque, P. 2007, *ApJ*, 655, 1166
- Pepe, F., Cameron, A. C., Latham, D. W., et al. 2013, *Nature*, 503, 377
- Pillitteri, I., Maggio, A., Micela, G., et al. 2015, *ArXiv e-prints*, arXiv:1503.05590
- Plavchan, P., & Bilinski, C. 2013, *ApJ*, 769, 86
- Rappaport, S., Joss, P. C., & Webbink, R. F. 1982, *ApJ*, 254, 616
- Rappaport, S., Sanchis-Ojeda, R., Rogers, L. A., Levine, A., & Winn, J. N. 2013, *ApJ*, 773, L15
- Rasio, F. A., & Ford, E. B. 1996, *Science*, 274, 954
- Rasio, F. A., Tout, C. A., Lubow, S. H., & Livio, M. 1996, *ApJ*, 470, 1187
- Reimers, D. 1975, in *Problems in stellar atmospheres and envelopes*, ed. B. Baschek, W. H. Kegel, & G. Traving (New York: Springer-Verlag), 229–256
- Ribas, I., Guinan, E. F., Güdel, M., & Audard, M. 2005, *ApJ*, 622, 680
- Rogers, L. A., Bodenheimer, P., Lissauer, J. J., & Seager, S. 2011, *ApJ*, 738, 59
- Sanchis-Ojeda, R., Rappaport, S., Winn, J. N., et al. 2014, *ApJ*, 787, 47
- , 2013, *ApJ*, 774, 54
- Sasselov, D. D. 2003, *ApJ*, 596, 1327
- Saumon, D., Hubbard, W. B., Burrows, A., et al. 1996, *ApJ*, 460, 993
- Schlaufman, K. C., & Winn, J. N. 2013, *ApJ*, 772, 143
- Sepinsky, J. F., Willems, B., Kalogera, V., & Rasio, F. A. 2010, *ApJ*, 724, 546
- Skumanich, A. 1972, *ApJ*, 171, 565
- Soberman, G. E., Phinney, E. S., & van den Heuvel, E. P. J. 1997, *A&A*, 327, 620
- Steffen, J. H., & Farr, W. M. 2013, *ApJ*, 774, L12
- Stevenson, D. J. 1979, *Geophysical and Astrophysical Fluid Dynamics*, 12, 139
- Teitler, S., & Königl, A. 2014, *ArXiv e-prints*, arXiv:1403.5860
- Teyssandier, J., Owen, J. E., Adams, F. C., & Quillen, A. C. 2015, *ArXiv e-prints*, arXiv:1504.01680
- Trilling, D. E., Benz, W., Guillot, T., et al. 1998, *ApJ*, 500, 428
- Valsecchi, F., & Rasio, F. A. 2014a, *ApJ*, 787, L9
- , 2014b, *ApJ*, 786, 102
- Valsecchi, F., Rasio, F. A., & Steffen, J. H. 2014, *ApJ*, 793, L3
- Verbunt, F., & Rappaport, S. 1988, *ApJ*, 332, 193
- Ward, W. R. 1997, *Icarus*, 126, 261
- Webbink, R. F. 1984, *ApJ*, 277, 355
- Weiss, L. M., & Marcy, G. W. 2014, *ApJ*, 783, L6
- Wu, Y., & Lithwick, Y. 2011, *ApJ*, 735, 109
- Wu, Y., & Murray, N. 2003, *ApJ*, 589, 605
- Zahn, J.-P. 1966, *Annales d'Astrophysique*, 29, 489
- Zahn, J.-P. 1977, *A&A*, 57, 383
- , 1989, *A&A*, 220, 112
- Zhang, M., & Penev, K. 2014, *ArXiv e-prints*, arXiv:1404.4365

Table 2
Summary of Results.

| M_c (M_\oplus) | γ | Σ_{pl} (g cm^{-2}) | Δt_{RLO} (Gyr) | P_{orb} at the end of RLO (d) | f at the end of RLO (%) | Δt when $f \sim 10\%$ to 20% (Gyr) | P_{orb} when $f \sim 10\%$ (d) | Δt when $f \sim 5\%$ to 10% (Gyr) | P_{orb} when $f \sim 5\%$ (d) | t when $f \sim 5\%$ (t_{MS}) | $t_{\text{RLO},2}$ (Gyr) |
|-------------------------|----------|--|----------------------------------|--|---------------------------------|---|---|--|--|---|-----------------------------|
| 5 | – | 1 | 6.9 | 3.8 | 37.7 | 1.3 | 3.8 | 0.4 | 3.8 | 1.1 | – |
| 10 | – | 1 | 6.9 | 1.7 | 39.6 | 1.0 | 1.6 | 0.2 | 1.3 | 1.1 | 10.9 |
| 15 | – | 1 | 6.6 | 1.2 | 35.9 | 0.6 | 0.9 | 0.2 | 0.7 | 1.0 | 10.3 |
| 30 | – | 1 | 5.7 | 0.3 | 1.0 | 0.3 | 0.5 | 0.1 | 0.4 | 0.8 | – |
| 5 | 0.6 | 1 | 3.7 | 3.5 | 40.1 | 2.0 | 3.5 | 2.8 | 3.5 | 1.1 | – |
| 10 | 0.7 | 1 | 3.4 | 1.6 | 43.8 | 1.7 | 1.6 | 2.5 | 1.5 | 1.0 | 10.9 |
| 15 | 0.7 | 1 | 3.6 | 1.2 | 43.7 | 1.5 | 1.0 | 1.1 | 0.8 | 0.9 | – |
| 30 | 0.7 | 1 | 3.1 | 0.3 | 1.0 | 0.3 | 0.5 | 0.1 | 0.4 | 0.5 | – |
| 5 | – | 100 | 7.2 | 4.2 | 37.6 | 1.1 | 4.2 | 0.1 | 4.2 | 1.1 | 10.9 |
| 30 | – | 100 | 6.2 | 0.4 | 1.0 | 0.3 | 0.6 | 0.1 | 0.5 | 0.8 | – |
| 5 | 0.6 | 100 | 3.7 | 3.9 | 40.8 | 3.0 | 3.9 | 1.6 | 3.9 | 1.1 | – |
| 30 | 0.7 | 100 | 4.0 | 0.4 | 1.0 | 0.3 | 0.6 | 0.1 | 0.5 | 0.6 | – |

Note. — The results include $M_{\text{env}}/M_{\text{pl}}$ values down to 5%, to allow a comparison between different MT assumptions and M_c values. In fact, for some of the models considered MESA does not converge when $M_{\text{env}}/M_{\text{pl}}$ drops below 5%. Time intervals are denoted with Δt . The parameters f , t , and $t_{\text{RLO},2}$ denote the envelope mass fraction ($M_{\text{env}}/M_{\text{pl}}$), the age of the system, and the time at which the planet undergoes a second RLO phase (if any), respectively. The first four examples are for conservative MT. For non-conservative MT we use $\delta = 1$ and vary γ as summarized in the second column. Note, the $30 M_\oplus$ core cases never detaches.